

## Intermonsoonal equatorial jets

P M Muraleedharan

Physical Oceanography Division, National Institute of Oceanography, Dona Paula, Goa-403 004, India

Received 25 March 1992; revised 21 October 1992

Three transects each from the cruises of *RV Pioneer* (84°, 88° and 92°E) during May-June 1964 and *RV Vityaz* (77°, 84° and 94°E) during October-November 1962 were used to compare pre and postmonsoon equatorial jets, respectively. Hydrographic features and transport computations favour a well developed equatorial jet during both seasons. The net surface eastward and subsurface westward flows are well balanced during the premonsoon transition period and appear to be decreasing from 84° to 92°E. In general, equatorial jet seems to be at its peak at 84°E irrespective of the season. Proximity of two opposing currents found one below the other during premonsoon within the equatorial jet would induce mixing, which may account for the vanishing of high salinity core that is otherwise associated with any eastward flow, and the formation of a layer of homogeneous water at the equator. Absence of similar phenomena, as in the case of postmonsoon transition, may preserve the structure of high salinity core.

Unlike in the other major oceans, in the Indian Ocean zonal circulation and near surface winds at the equator reverse several times annually<sup>1</sup>. Wyrki<sup>2</sup> first noticed the organisation of winds at the equator into moderate westerlies between the monsoons, especially in central and eastern equatorial Indian Ocean. O'Brien and Hurlburt<sup>3</sup> successfully developed a two-dimensional numerical model to explain the salient features reported by Wyrki<sup>2</sup>.

Subsequently a systematic observation of the jet was carried out by Knox<sup>4</sup> using uninterrupted time series data on both wind and surface current for about 2y collected at Gan (73°E) in the Maldivian group of Islands. He recorded the appearance of the jet in the thermocline as well as at the surface, with speeds exceeding 100 cm.sec<sup>-1</sup>. During the fall of 1980 another attempt was made to track the jet for about 3000 km using satellite linked drifting buoys<sup>5</sup>. This time the width of the jet never exceeded 2° on either side of the equator.

Very few attempts have been made to study the occurrence of jet in the western Indian Ocean (west of 73°E). Although the observation of Luyten *et al.*<sup>6</sup> indicates a jet at 62°E from May to June 1979, the complicated vertical current structure does not support the conventional concept of an Equatorial Jet as stated by Wyrki<sup>2</sup>. This appears to be favouring the views of Philander<sup>7</sup> who believes that non-linear effects are important on time scales longer than about one week and

that winds that fluctuate on such time scales introduce hysteresis effects and generate flow with a complicated vertical structure. Similar effects have also been noticed by Luyten & Swallow<sup>8</sup> at 55°E during May-June. However Leetma & Stommel<sup>9</sup> have reported the absence of persistent or strong westerlies at 55.30°E during the transition periods in 1975 and 1976. They have presumed that Wyrki's<sup>2</sup> jet might develop further to the east where historical data showed the westerlies to be stronger.

In view of the conflicting reports, an attempt has been made to work out the hydrography and mass transport of the jet in the central and eastern equatorial Indian Ocean during 2 transition periods with the available data set.

### Materials and Methods

Hydrographic data collected during IIOE (1960-1965) along 84°, 88° and 92°E in May-June 1964 and 77°, 84° and 94°E (Fig. 1) during October-November 1962 by *RV Pioneer* and *RV Vityaz* during their 442 and 35 cruises, respectively, were procured from National Oceanographic data center at N.I.O. Goa, India for the present study. To facilitate an easy comparison of the distribution of hydrographic properties, each set of diagrams is superimposed and represented with different types of notation. The isotherms and isohalines are drawn with an interval of 1°C temperature and  $0.1 \times 10^{-3}$  salinity, respectively. As the equatorial current system is con-

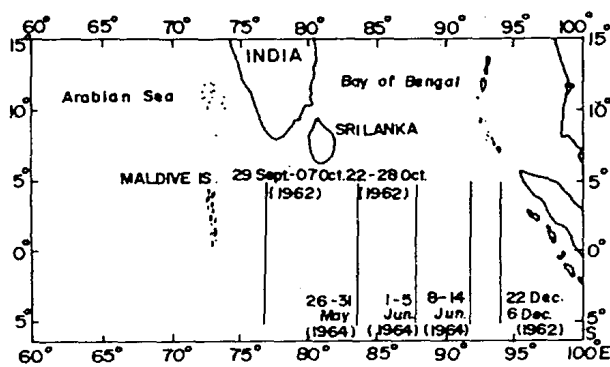


Fig. 1 - Cruise track and area of study [thick lines indicate transects covered during the pre- and postmonsoon transition periods]

fined to a maximum depth of 300 m, the analyses were restricted to upper 300 m layer between 5°N and S.

**Computation of zonal flux**—The real ocean is always baroclinic and as a result the isobaric and isosteric surfaces intersect at an angle, producing a lateral density gradient. This density gradient causes circulation which is a tendency to adjust the mass distribution closer to that of static equilibrium in order to establish barotropic mass field. Since the horizontal displacement of water takes place along the steric surface, the velocity field is computed in each steric level rather than depthwise. This appears to be more appropriate and reliable. The first attempt to compute the geostrophic volume flux from acceleration potential at each steric level was made by Montgomery & Stroup<sup>10</sup>. By dividing the flux into bivariate classes defined by thermosteric anomaly and salinity, they successfully estimated the zonal geostrophic transport in the Pacific Ocean. Masuzawa<sup>11</sup>, after certain modifications, used the same method for estimating zonal geostrophic flux in the Pacific Ocean along various longitudes. Later Cochrane *et al.*<sup>12</sup> followed the same technique to estimate zonal transport of the Subthermocline Countercurrent in the Equatorial Atlantic Ocean.

The method to compute volume transport, introduced by Montgomery & Stroup<sup>10</sup> gives the function  $\phi_a + p\delta$  at chosen isanosteric surfaces. The symbol  $\phi_a$  stands for anomaly of geopotential, relative to the reference surface (here the level of no motion is assumed at 1000 m),  $p$  for sea pressure and  $\delta$  for specific volume anomaly. The function  $\phi_a + p\delta$  has been called acceleration potential<sup>13</sup>. This function is simpler to calculate than alone. This method directly estimates the geostrophic current at chosen isanosteric surfaces. The

anomaly of geopotential is defined by an integral along a vertical line.

$$\phi_a = \int_p^{p_0} \delta dp$$

where  $p_0$  is the reference pressure (pressure at 1000 m depth). Changing the variable of integration leads to acceleration potential.

$$\phi_a + p\delta = p_0\delta_0 + \int_{\delta_0}^{\delta} p d\delta$$

where  $p_0$  is the specific volume anomaly at the reference pressure. Since the pressure in the upper 300 m is negligible the anomaly of specific volume is now replaced by thermosteric anomaly, ( $\delta_T$ ), and  $\phi_a$  and  $\phi_a + p\delta$  are modified correspondingly.

The numerical integration has been carried out at each whole degree of latitude, to yield the acceleration potential at chosen standard isanosteres and at the sea surface (where  $p = \theta$  and  $\phi_a + p\delta$  reduces to  $\phi_a$ )

Now the geostrophic velocity takes the form

$$v = (\phi_A - \phi_B) / 2\Omega L \sin \theta$$

where  $\phi_A$  and  $\phi_B$  are the acceleration potential at stations A and B, respectively,  $L$  is the distance between the stations,  $\Omega$  the angular velocity and  $\theta$  the mean latitude.

To compute geostrophic volume flux through each vertical meridional quadrangle formed by 2 successive whole degrees of latitude and 2 successive standard isanosteres, the vertical profile of velocity is superimposed by the vertical section of thermosteric anomaly. If the mean length and thickness of each quadrangle and the velocity of water flowing through it are known, the volume of water flowing through it (flux) can be calculated.

In order to study the water characteristics within the jet, the total transport/flux is distributed in different classes of thermosteric anomaly and salinity. The dimension of each class is 40  $\text{cl.t}^{-1}$  thermosteric anomaly and  $0.2 \times 10^{-3}$  salinity. This is achieved by superimposing salinity section with that of flux. Net transport is then computed and displayed for each characteristic class, with intervals of 40  $\text{cl.t}^{-1}$  in thermosteric anomaly and  $0.2 \times 10^{-3}$  salinity. The total flux between any 2 consecutive intervals of thermosteric anomaly is

shown at the top and that of salinity on the right hand side of the diagrams.

## Results

*Analysis of hydrographic fields*—The processes occurring in the surface layer of the ocean are remarkably controlled by the distribution of temperature while the part played by salinity is less significant in inferring the phenomena occurring at the surface. Therefore the equatorial jet in the Indian Ocean is inferred mainly from the distribution of temperature alone. The contrasting east-west salinity gradient in the equatorial Indian Ocean makes it possible to trace the jet (eastward flow) right from the central Indian Ocean to Sumatra coast at the east. This also provides supplementary information on the jet.

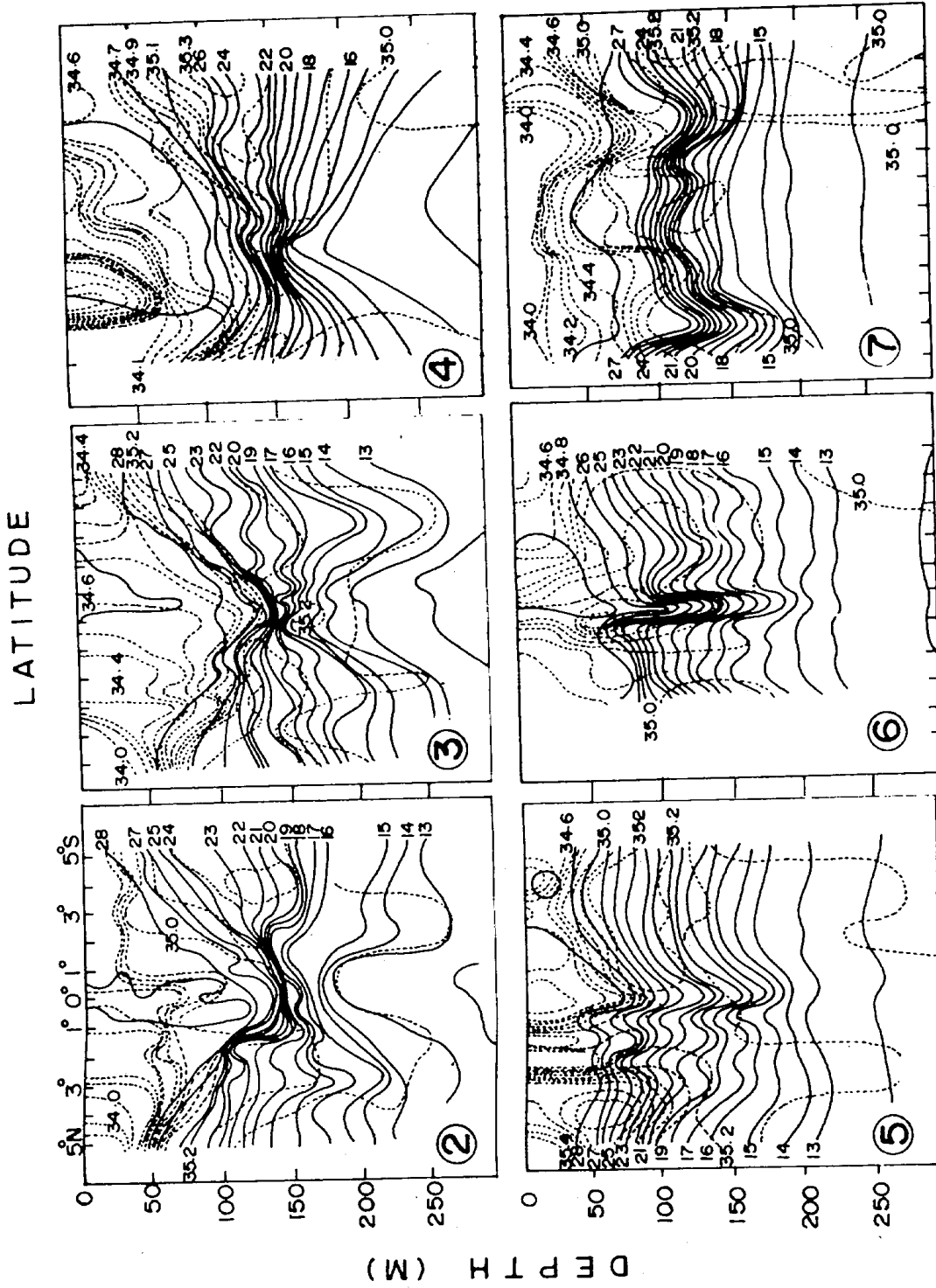
*Premonsoon transition period (May-June)*—Sections of temperature along 84°, 88° and 92°E depict a similar pattern of isotherms, compressed at the equator and spreading vertically towards poles. The intensity of the gradient of isotherm at the equator appears to weaken from central (84°E) to the eastern equatorial Indian Ocean. The troughing of isotherms at the surface layer is more pronounced at 84°E and tends to be shallow at 92°E. The ridging of isotherms in the subsurface layer is more or less consistent in all transects. The convergence of isotherms is symmetrical about the equator along 84°E and 88°E but it is asymmetric at 92°E. The region of highest gradient at this longitude shifts to the northern hemisphere.

All transects here indicate similar distribution of salinity, having high salinity tongue penetrating towards the equator from both hemispheres (Figs. 2-4). The very low salinity patch at 3°N, visible at extreme east (92°E), drifts towards the equator from far north (5°N) (Figs. 2 and 3) as the jet travels from 84° to 92°E. The deepening of isolines of salinity at 84° and 88°E towards the equator may be an indication of downward transport of momentum which is supposed to be associated with the equatorial jet. The absence of similar phenomena at 92°E, together with the uplifting of the isohalines at the equator (Fig. 4) probably indicates vertical transport of momentum associated with the westward subsurface flow as the surface jet loses its characteristics and appears to drift towards north. The subsurface high salinity tongue from the south penetrates across the equator while the one from the north withdraws to 5°N.

*Postmonsoon transition period (Oct.-Nov.)*—Thermal and saline structure in the upper 300 m layer during this period does not show any similarity with the previous sections. Remarkable changes in the topography of isotherms are detected from one section to the other. When the isotherms exhibit wavy amplitudes at 77°E, they show intense troughing in the vicinity of the equator at 84°E. However, the pronounced troughing near the equator at both 77° and 84°E could be the manifestation of the jet, whereas the apparent doming of the upper thermocline at 94°E might be associated with an opposite flow. Unlike in the previous figures (Figs. 2-4) the topography of subsurface isotherms at 77°, 84° and 94°E runs more or less parallel to the surface (Figs. 5-7).

The surface salinity at 77°E decreases from 5°N to 5°S (Fig. 5). A high salinity core ( $> 35.8 \times 10^{-3}$ ) is observed near 4°N in the subsurface layer (~50-100 m) which appears to be advecting towards the equator. Similarly penetration of saline water from south towards the equator is also noticed around the same depth. Further east (84°E) a well defined high salinity core appears at 1°N whose vertical extent coincides with the intense troughing in the isotherms (Fig. 6). At 92°E the thermocline and halocline are distinctly separated to lie one over the other. A feeble high salinity core still survives below 100 m at the equator (Fig. 7).

*Distribution of net transport*—Zonal transport within equatorial jet is computed across 84°, 88° and 92°E during the premonsoon transition period (May-June) and across 77°, 84° and 94°E during postmonsoon transition period (October-November), following Montgomery & Stroup<sup>10</sup>. The transport is computed between 3°N and S as the width of the jet never extended beyond these latitudes<sup>2,3,14</sup>, although the distribution of properties spreads up to 5°N and S. Hereafter, PRT and PST indicate, respectively, pre and postmonsoon transition periods. Table 1 gives zonal transport computed across 6 meridional sections. It is evident from the frequency distribution of transport (Figs. 8-13) that in most of the transects, >50% of the eastward transport lies in the surface layer while the westward transports is restricted to deeper layer except at 94°E during PST. The eastward and westward transports during PRT exhibit high resemblance in magnitude and seem to be consistently decreasing from 84° to 92°E whereas the transport during PST indicates an increase in eastward flux from 77° to 84°E and then suddenly vanishes as it approaches 94°E. The westward transport during this season, however, picks up



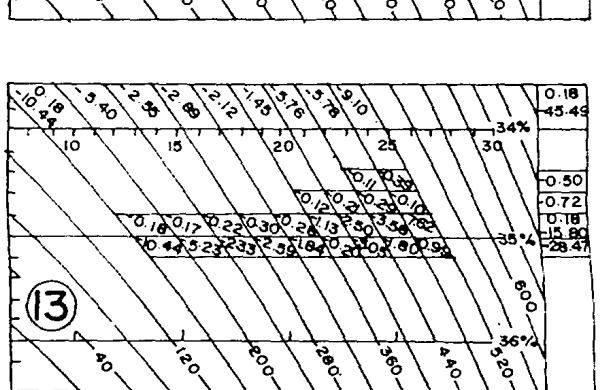
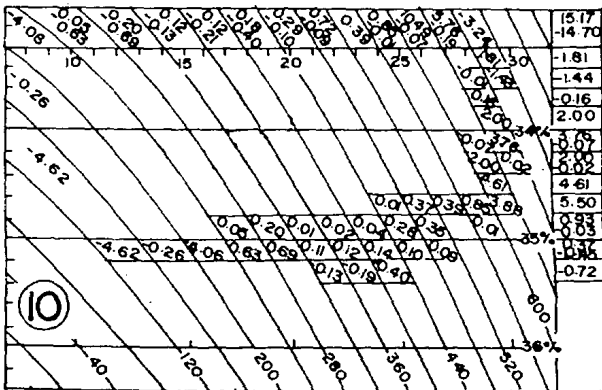
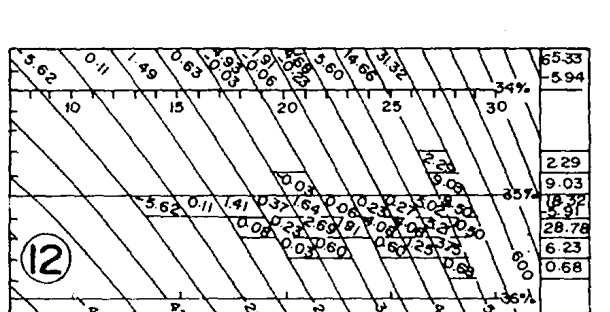
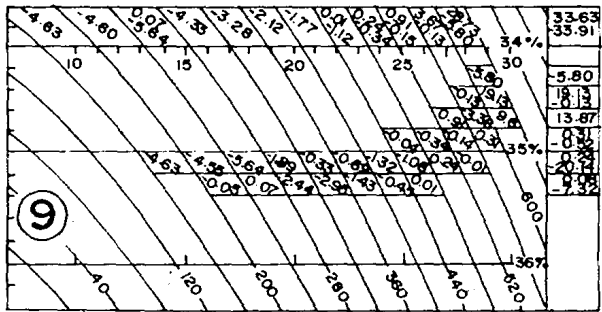
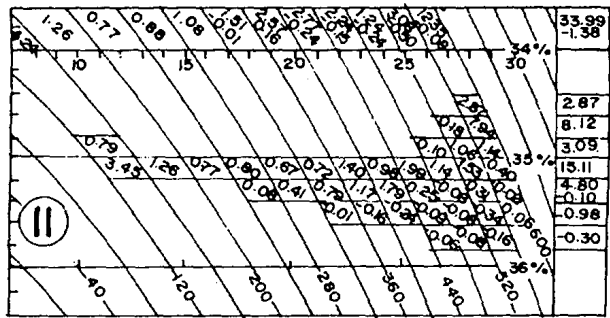
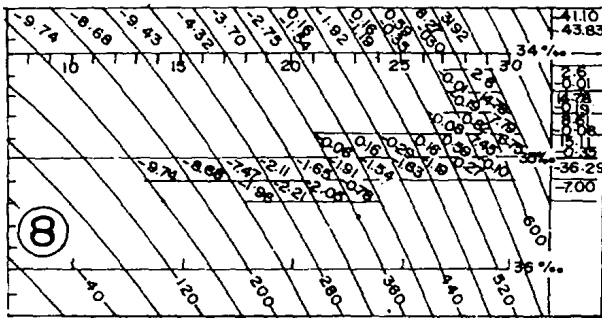
Figs. 2 to 7 - Vertical distribution of temperature (solid line) and salinity (broken line) along 84°E in May (2), 88°E in June (3), 92°E in June (4), 77°E in September-October (5), 84°E in October (6), and 94°E in November-December (7).

dramatically from 1.38 sv (1 svedrup =  $10^6 \text{m}^3 \cdot \text{s}^{-1}$ ) to 45.49 sv within a span of 1870 km (17 degrees) (Table 1). The high eastward transport appears to be associated with 84°E during both PRT and PST (Table 1).

*Bivariate distribution of zonal transport*—Transport values across each transequatorial section are distributed in a number of classes (frequencies) defined by thermosteric anomaly and salinity to facilitate representation on a temperature-salinity-delta-T diagram (Figs. 8-13). Frequency distribution of the westward transport is not discussed here as it is irrelevant to the present context. The values enclosed by solid lines are of those classes

Table 1—Transport ( $\text{sv} = 10^6 \text{m}^3 \cdot \text{sec}^{-1}$ ) computed across 6 meridional transects during pre- and postmonsoon transition (PRT and PST respectively) periods

Long.	PRT		Long.	PST	
	Transport (sv)			Transport (sv)	
	Eastward	Westward		Eastward	Westward
84°E	41.10	43.83	77°E	33.99	1.38
88°E	33.63	33.91	84°E	65.33	5.94
92°E	19.17	14.70	94°E	00.18	45.49



Figs. 8 to 13—Distribution of the net transport across 84°E during May (8), 88°E during June (9), 92°E during June (10), 77°E during September-October (11), 84°E during October (12) and 94°E during November-December (13), in bivariate classes of thermosteric anomaly and salinity. The solid-line boundary encloses classes that together contribute 50% of the transport; the dashed-line boundary encloses classes that contribute 75%. The totals at the top of the figure give distribution by thermosteric anomaly and those on the right, by salinity. The total in the box in the top right-hand corner gives total transport (sv). Negative values indicate westward transport.

that together contribute 50% of total transport and are said to be within the 50% boundary. Similarly, 75% boundary (dashed line) is defined as that which encloses transport values of classes that contribute 75% of total transport. These diagrams, besides giving bivariate distribution of salinity and thermocline anomaly at intervals of  $0.2 \times 10^{-3}$  and  $40 \text{ cl.t}^{-1}$  respectively, also give the temperature variation as the isanosteric surfaces is dependent only on temperature and salinity. Therefore, for any single salinity interval there is bound to be only a single temperature interval. By comparing interval of temperature with the corresponding diagram of distribution of temperature, it is possible to delineate the depth distribution of each frequency. Table 2 shows the number of frequencies enclosed by the 50 and 75% boundaries in all the sections investigated.

The difference in the number of frequencies between 50% and 75% levels (Table 2) during two transition periods is a manifestation of the characteristics of the water mass within the jet. The frequencies enclosed by 50% boundary at  $84^\circ$  and  $88^\circ\text{E}$  are only 2 and 1, respectively, and an increment of one frequency accounts for a 25% increase in transport. This increment is remarkably high during PST, especially at  $77^\circ\text{E}$ . The solitary frequency observed at  $94^\circ\text{E}$  (Fig. 13) represents insignificant amount of transport (0.18 sv) and hence is excluded from the discussion. The sum of all frequencies belonging to a particular season is termed in the table as total frequency. The total frequency in the 50% boundary is much less when compared to that in the 75% level during the PST. The additional 12 frequencies are accounted for by the 25% increase in the transport. In the 50% level the PST has 9 total frequencies, which is comparatively higher than its premonsoon counterpart (6 frequencies). The difference in total number of frequencies between 50 and 75% boundaries is more during PST (12 frequencies) than PRT (4 frequencies), despite the fact that the transport at  $94^\circ\text{E}$  during PST is too small to occupy more than one frequency (Table 1). A

close examination of the frequencies (Table 2) between  $80^\circ$  and  $90^\circ\text{E}$  indicates a marginal increase from 50 to 75% boundary, especially during PRT.

### Discussion

The well known seasonal fluctuation in wind speed and direction in the Indian Ocean manifests as the southwest and northeast monsoons over the Arabian Sea, Bay of Bengal and the Indian subcontinent. Along the equator the variation is quarterly, resulting in the development of a strong eastward flowing current called equatorial jet<sup>2</sup> during the 2 transition periods between monsoons. Since its discovery very few observations have been made at the equatorial Indian Ocean<sup>4,5,15</sup> with a view to understand this unique feature. These observations have the limitation of coverage in space as well as time, as the jet often makes its appearance during both pre and post-monsoon transition periods and also from central to eastern part of equatorial Indian Ocean. In view of this fact, the data set collected during the International Indian Ocean Expedition (IIOE) much before the discovery of the jet continues to be relevant.

Hydrographic section depicts the distinct behaviour of these intermonsoonal jets especially at  $84^\circ\text{E}$  where repeated coverage of the transect is available during both transition periods (Figs. 2 and 6). The thermal structure during PRT shows a thermocline compressed at the equator and spreading vertically on either side, indicating an intense eastward flow at the surface with an equally strong subsurface opposite flow (Figs. 2 and 3). Although the hydrography at  $77^\circ$  and  $84^\circ\text{E}$  during PST favours a surface jet, it shows no indication of a reverse flow at the subsurface depth.

The net eastward transport (jet) at the surface layer and westward transport in the subsurface layer (Table 1) are highly comparable in magnitude and appear to be consistently decreasing from  $84^\circ$  to  $92^\circ\text{E}$  during PRT. It is surprising to note the co-existence of 2 opposite currents one over the other (Figs. 2 and 3), transporting an almost equal volume of water (Table 1). These two zonal currents flowing along the equator can cause vertical transports of momentum<sup>16</sup>, one downward and the other upward, inducing mixing at the equator. In the absence of one of these currents, as in the case of PST (Figs. 5 and 6), the mixing is less pronounced and the system is incapable of producing the kind of thermal structure found during PRT (Fig. 2). At this stage it is fairly logical to conclude from the transport com-

Table 2 - Number of frequencies enclosed by 50 and 75% boundaries at 6 meridional transects

Boundary	PRT (May-June)			Total	PST (Oct.-Nov.)			Total
	84°E	88°E	92°E		77°E	84°E	94°E	
50%	02	01	03	06	04	04	01	09
75%	03	02	05	10	12	08	01	21

putation that the intensity of the jet reaches a maximum at 84°E and then starts weakening. During postmonsoon transition season the jet vanishes at 94°E and a strong westward transport appears at the subsurface depth (Table 1).

The contrasting salinity structures of the Arabian Sea and the Bay of Bengal always make it easy to trace a zonal flow at the equator. Normally the equatorial jet carries high saline water from west to east. Although the high salinity tongues appear to be penetrating towards the equator from both hemispheres during PRT (Figs. 2 and 3), they fail to meet at the equator to form the core as in the case of the transect at 84°E covered during PST (Fig. 6). This is due to the fact that the proximity of 2 opposing currents present one below the other creates stress which would ultimately generate severe mixing at the boundary of these currents, as seen earlier. The result is the disappearance of high salinity core and formation of a layer of homogeneous water within the equatorial jet.

For added confirmation of the above facts it may be worthwhile to examine the frequency distribution of transport across the transects under investigation. In Table 2, 50% of transport during PRT is represented by a solitary frequency at 88°E and by 2 frequencies at 84°E; an additional frequency accounts for the remaining 25% transport. At the same time the frequency occupied by the 75% boundary during PST is twice that of the 50% level at 84°E and 3 times at 77°E. This indicates the level of homogeneity of water close to the equator during PST and PRT. The less homogeneous water mass observed during PST indicates a weak mixing at the equator which could retain the structure of the high salinity core. The

water mass of the upper 300 m layer close to the equator appears to be more homogeneous during PRT than PST in both 50 and 75% levels. In general, water in the surface layer between 80° and 90°E tends to become homogeneous with respect to surrounding water, irrespective of the season. This information reiterates the earlier conclusion of an intense surface jet at 84°E during both transition periods.

## References

- 1 Anonymous, Koninkrijk Netherlands Meteorologisch Instituut, Indische Ocean Oceanografische en Meteorologische gegevens, Publ No. 135, 1952, pp. 31.
- 2 Wyrtki K, *Science* 181 (1973) 262.
- 3 O'Brien J J & Hurlburt H E, *Science*, 184 (1974) 1075.
- 4 Knox R A, *Deep-Sea Res*, 23 (1976) 211.
- 5 Cresswell G, Fieux M & Gonella J, *Tropical Ocean-Atmosphere Newsletter*, 1981.
- 6 Luyten J R, Fieux M & Gonella J, *Science*, 209 (1980) 600.
- 7 Philander S G H, *J Phy Oceanogr*, 9 (1979) 739.
- 8 Luyten J R & Swallow J C, *Deep-Sea Res*, 23 (1976) 1005.
- 9 Leetma A & Stommel H, *J Phy Oceanogr*, 10 (1980) 258.
- 10 Montgomery R B & Stroup E D, *Equatorial waters and currents at 150°W in July-August 1952*, (John Hopkins, Oceanogr Stud.) 1962, pp. 68.
- 11 Masuzawa J, *Stud Oceanogr* (Tokyo), (1964) 121.
- 12 Cochran J D, Kelly F J & Olling C R, *J Phys Oceanogr*, 9 (1979) 724.
- 13 Montgomery R B & Spilhaus A F, *J Aeron Sci*, 8 (1941) 276.
- 14 Fieux M & Gonella J, *Drifting buoy trajectories in the Equatorial Indian Ocean*. Recent Progress in Equatorial Oceanography - A report of the final meeting of SCOR working group 47 (Venice, Italy), 1981.
- 15 Reverdin G, Fieux M, Gonella J & Luyten J, in *Proceedings of the 14th International Liege Colloquium on Ocean hydrodynamics* 1983, pp. 99.
- 16 Cane M A, *Deep-Sea Res*, 27 (1980) 525.